12

Analysis of beam orbit stability at the skif

© G.N. Baranov,[1,2,3] P.A. Dergach,[4,5] K.Yu. Karyukina,[1,2] V.A. Pavliuchenko,[2] E.B. Levichev[1,2,3]

[1] Resource Sharing Center „The Siberian Circular Photon Source“
Boreskov Catalysis Institute, Siberian Branch, RAS,
630559 Koltsovo, Russia
[2] Budker Institute of Nuclear Physics, Siberian Branch, Russian Academy of Sciences,
630090 Novosibirsk, Russia
[3] Novosibirsk State Technical University,
630073 Novosibirsk, Russia
[4] Trofimuk Institute of Petroleum Geology and Geophysics, Siberian Branch RAS,
630090 Novosibirsk, Russia
[5] Novosibirsk State University,
630090 Novosibirsk, Russia
e-mail: K.Yu.Karyukina@inp.nsk.su

Received June 21, 2023
Revised September 4, 2023
Accepted September 4, 2023

The Resource Sharing Centre “The Siberian Circular Photon Source“˜„SKIF“) — is a fourth-generation synchrotron radiation (SR) source currently under construction in Novosibirsk. Ensuring the mechanical stability of the magnetic elements of a modern SR source is a complex and important task, since even small displacements of magnets relative to the design position, caused, among other things, by seismic vibrations of the construction site surface, can significantly degrade the installation parameters. The article presents the results of a study of the seismic situation in the area of the construction site of the „SKIF“, the main sources of the seismic background are identified and, based on the data obtained, the parameters of the feedback system are estimated, which allows dynamically adjusting the position of the electron beam at radiation points, stopping the negative impact of seismic effects on the efficiency of the SR source work.

Keywords: synchrotron radiation source, emittance, stability of magnetic elements, synchrotron radiation brightness, seismic vibrations.

DOI: 10.61011/TP.2023.11.57506.153-23

Introduction

Modern synchrotron radiation (SR) sources — are ultra-relativistic energy (up to several gigaelectronvolts) electron accelerators (storage rings) . accelerated beam moves in the transverse magnetic field and emits photons tangentially to the motion path. Having a set of unique properties, this radiation is widely used in various research and development areas.

Radiance defined as a photon flux normalized to the source phase volume (emittance) is one of main parameters of the SR source that characterizes its „quality“. To improve the radiance, emittance of the storage rings is optimized by „compressing“ the particle beam using powerful focusing (quadrupole) lenses. Magnetic field of the quadrupole lens is equal to zero axially and grows linearly with increasing transverse coordinate of the particle. When quadrupole lenses move transversely for whatever reason, then dipole fields occur on the orbit that divert the beam as a whole and cause both angular and coordinate displacements of the electron beam (and, thus, of the SR beam) in the radiation point. If the period of such displacements (mechanical vibrations) of quadrupole magnets is shorter than the typical exposure time, then SR beam „jitter“õn the sample or optical elements will result for the researcher in an increase in effective phase volume of the source and decrease in radiance. This is also true for any other magnet with transversely inhomogeneous field.

In the Gaussian approximation, the undulator radiance peak is calculated as:

$$Br \propto \frac{1}{\sqrt{\sigma_x^2+\sigma_u^2}\sqrt{\sigma_{x'}^2+\sigma_{u'}^2}\sqrt{\sigma_y^2+\sigma_u^2}\sqrt{\sigma_{y'}^2+\sigma_{u'}^2}}, \quad (1)$$

where$\sigma_{x,y}$ and $\sigma_{x',y'}$ are electronic size of the beam and divergence in the horizontal and vertical planes in the radiation point, σ_u and $\sigma_{u'}$ are the beam size and radiation divergence. Typical transverse sizes of the electron beam in the radiation points achieve several microns, and the allowable orbit displacement is 5−10% from these values. Horizontal emittance of the electron beam will be 73 pm · rad, while the vertical emittance with 10% bond will be 7.3 pm · rad. Rms size and divergence of the radiation source for a single electron in the undulator depend on the radiation wavelength λ and are defined as $\sigma_u = \sqrt{2\lambda L}/4\pi$, $\sigma_{u'} = \sqrt{\lambda/2L}$, where L is the undulator length. Thus, for a single electron in the undulator at 10 Å radiation phase volume is equal to 80 pm · rad, at 1 Å — is already equal

to8 pm · rad, that is comparable with the vertical emittance of the electron beam.

Since the quadrupole lense displacement transforms into the beam displacement with amplification of several tens of times (due to strong-focusing optics of the SR source required to minimize the emittance), the ring magnet deviation amplitude tolerance in the low frequency region is equal to only tens of nanometers, and mechanical stability of magnetic elements shall be given very serious consideration when designing modern SR sources.

There is a great variety of magnetic element microvibration sources for the storage ring. These may include earthquake activity, microseims of both natural and man-made origin, seismic background of production facilities (in particular, mining), major transportation routes (railways, tramways, highways) in the immediate vicinity of the SR source, etc. Seismic noise may be induced by the engineering infrastructure of a plant — transformers, pumps, lifting gear, etc. Finally, microvibration sources may occur directly on the magnets — for example, this may be a turbulent liquid flow in cooling tubes of current windings that excite the magnetic field.

To meet the stringent requirements for spatial stability of magnetic components, various measures are taken, including the selection of construction site in a low seismic activity zone far from industrial regions and large transport systems (which not always possible), complex seismic damping foundation engineering. Magnetic components are placed and secured rigidly in groups on dedicated girders by choosing the components in such a way that their coherent motion has a lower effect on the beam displacement than the self-motion. Mechanical structures (magnets + girders) are optimized in such a way as to make their lowest resonant vibration modes higher by frequency than the typical excitation sources, whereby, at high frequencies, mechanical frequencies shall not coincide with the excitation frequencies. Finally, an active feedback system is provided, including (electron and photon) beam position sensors and weak alternating gradient magnetic adjusters arranged in such a way as to have the maximum effect on the beam in the radiation point.

Important tasks at the SR design stage include seismic background examination at the construction site, risk identification and assessment of various seismic sources, and preliminary design of the beam vibration correction system based on the examination findings. These issues are discussed herein.

1. „SKIF“ synchrotron radiation source

Resource Sharing Center „The Siberian Circular Photon Source“ (RSC „SKIF“) — fourth-generation SR source — is a complex accelerating system consisting of a 200 MeV beam energy linear accelerator, booster synchrotron (maximum energy is 3 GeV), storage ring (3 GeV) [1] and six experimental first-stage stages (Figure 1).

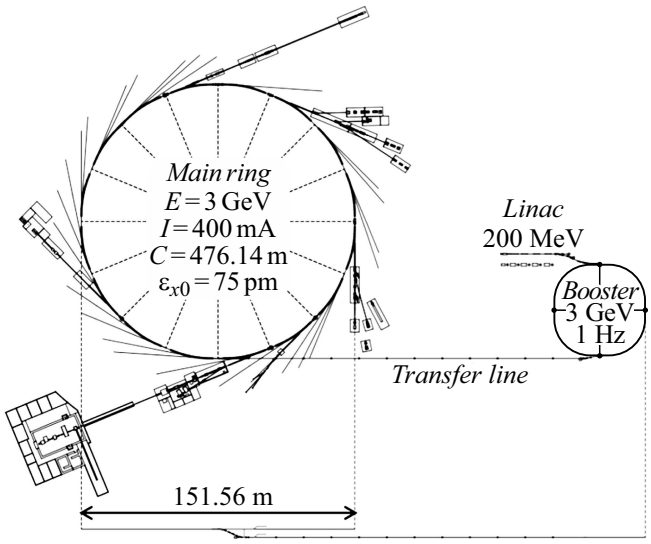

Figure 1. Main plant layout of RSC „SKIF“. Linear accelerator, booster synchrotron, main electron storage ring and several experimental stations are shown. E is the beam energy, I is the current, C is the ring perimeter, ε_{x0} is the horizontal natural emittance.

Table 1. Specifications of RSC „SKIF“ 3 GeV booster and storage ring

Description	Booster	Storage ring
Energy, GeV	3	3
Perimeter , m	158.71	476.14
Periodicity	4	16
Horizontal emittance, pm · rad	37 400	73
Energy spread, %	$8.3 \cdot 10^{-4}$	$1.3 \cdot 10^{-3}$
Betatron frequencies(x/y)	9.65/3.41	50.81/18.84
Orbit compaction coefficient	$8.8 \cdot 10^{-3}$	$7.6 \cdot 10^{-5}$

The main specifications of the plants are listed on Table 1 and are used below for various estimates. Since the beam emittance in the storage ring is much lower than in the booster, it is apparent that the mechanical stability requirements for the storage ring equipment are much more stringent than for the synchrotron–booster.

SKIF storage ring consists of sixteen identical achromatic superperiods with 7MBA (Multiple Bend Achromat) [2] type magnetic structure, each of them has a straight end section 6 m in length. Fourteen sections are intended to install removable radiating devices (multipole magnetic wigglers and undulators), and the remaining two sections are intended to install injection equipment and high-frequency accelerating resonators.

To achieve low emittance, it is necessary to use weak bending magnets with small angle of rotation θ (since$\varepsilon_x \propto \theta^3$) that have soft X-ray and vacuum-UV radi-

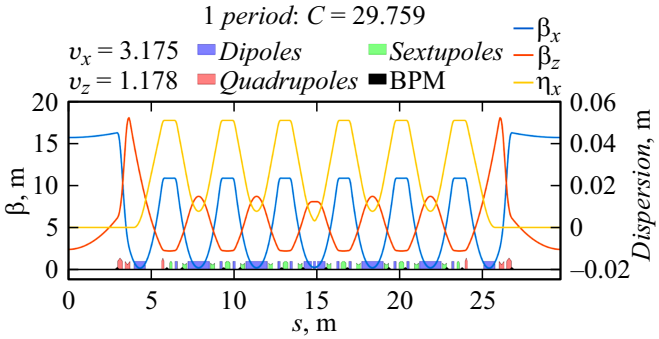

Figure 2. Optical functions of the storage ring superperiod. ν_x, ν_z are horizontal and vertical betatron frequencies (dimensionless quantities), C is the superperiod length, [m], s is the longitudinal coordinate along the superperiod, β_x, β_z is the horizontal and vertical beta functions, [m], η_x is the horizontal dispersion function, BPM — Beam Position Monitor.

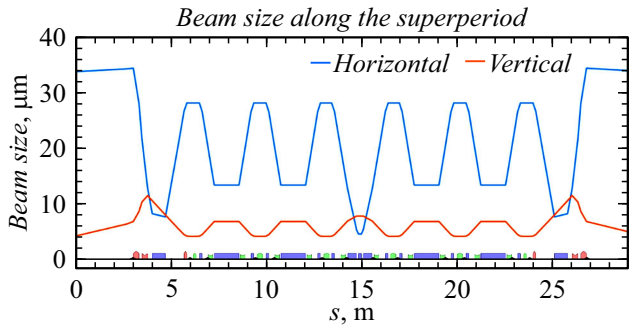

Figure 3. Dependence of rms beam sizes along the SKIF superperiod. s is the longitudinal coordinate along he superperiod.

ation spectra. To meet the user demands for rigid X-ray range, the central magnet in each superperiod is separated with a strong-field insert — a dipole on powerful permanent NeFeB magnets that provide a 2.1 T field on the orbit. Most of dipole magnets that form a closed beam orbit contain a transverse field gradient and are involved in the focusing process to ensure more space-saving structure [1].

Optical functions of one superperiod are shown in Figure 2. Electron beam rms sizes and divergences along the superperiod calculated as ollows

$$\sigma_y = \sqrt{\varepsilon_y \beta_y}, \quad \sigma_x = \sqrt{\varepsilon_x \beta_x + \eta_x^2 \delta^2}, \qquad (2)$$

where $\varepsilon_{x,y}$ is the beam emittance, $\delta = \Delta E / E_0$ is the energy spread in the beam, η_x is the dispersion function, and $\beta_{x,y}$ betatron function shown for one superperiod in Figure 3.

Beam rms sizes and rms angular divergence in points of radiation emission from the straight section and strong-field magnet are listed in Table 2.

Minimum (vertical) rms beam size (1σ) in the center of the straight section — about $4\,\mu$m. The accepted beam stabilization positioning tolerance — is $< 10\%$ of the beam size in the radiation point [3] ($\sim 3-5\%$ is achieved

Table 2. Space and angular beam dimensions in radiation emission points

Radiation emission point	σ_x, μm	$\sigma_{x'}$, μrad	σ_y, μm	$\sigma_{y'}$, μrad
Removable source	33.7	2.2	4.2	1.7
Dipoles	5.7	22.8	7.7	1

actually), and this means that the feedback system shall ensure beam stability in this point with accuracy better than $0.4\,\mu$m for „uncontrolled“ seismic vibration sources on the surface of RSC „SKIF“ construction site. It is assumed that the noise from the „controlled“ sources inside the SKIF building (pumps, transformers, ventilation and air conditioning systems, handling systems, etc.) may be minimized using vibration-reducing solutions in the structure and hardware.

2. Investigation of seismic vibrations on the RSC „SKIF“

Analysis of soil vibrations effect is an integral part of design of modern synchrotron radiation sources [4–7]. Detailed seismic environment analysis of the RSC „SKIF“ site was performed by Altai-Sayan branch of Federal Research Center „Unified Geophisical Service of Russian Academy of Sciences“ and by Trofimuk Institute of Petroleum Geology and Geophysics, Siberian Branch RAS.

The measurements were carried out by the three-component seismic station network (Figure 4) during the period from 01.11.2021 to 11.01.2022. Five stations

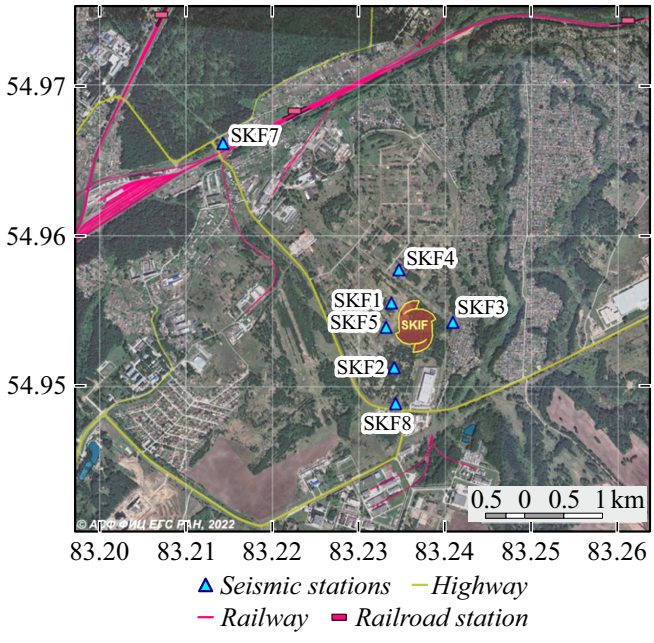

Figure 4. RSC „SKIF“ local seismic station network (blue triangles (in online version)).

Table 3. Classification of seismically relevant events on the RSC „SKIF“ site

Events	Number per 24 hours	f, Hz	t, s	PGA, μm/s^2	PGV, μm/s	PGD, μm	RMS, nm
Earthquakes	0.3	5–20	15–200	150–1300	5–25	3–9	500
Industrial explosions	1.6	5–20	15–25	250–1700	5–25	1–3	500
Railway transport	100	3–8	200	100–2500	3–60	1–3	100–300
Road transport	2500	5–30	10–30	< 2500	< 40	≤ 1	60–200
Industrial segment	–	20–50	–	–	–	–	–
Noise (day/night)	–	2–100	–	1000/100	50/5	0.15/0.02	35/5

were located directly on the site, and two stations were placed near the railway and highway to examine seismic wave attenuation. An additional set of measurements by a lower number of stations (three) was performed for independent check. Results of both measurements are in good agreement.

Brief summary of the measurements [8]:

• A total of 2140 seismic events were recorded during almost two months of observations in the radius of 500 km from RSC „SKIF“ 648 of them are classified as earthquakes (including man-made) and 1456 are classified as industrial explosions. Only 24 of these events have local magnitude ML ≥ 3. Minor and distant earthquakes have a frequency spectrum not exceeding 4–5 Hz and small amplitude, major earthquakes extend on the spectrum up to 20–30 Hz and have a larger vibration amplitude, but are extremely rare. Industrial explosions in the nearby (~ 50 km) quarries have a wide spectrum, but are very short-term and more likely pose no hazard to the experiment.

• Seismic loads from the railway transport are defined as a set of multiple harmonics covering a wide frequency range from ~ 3–6 Hz and higher. Primarily freight trains have noticeable impact (up to peak soil displacements PGD $= 3\,\mu$m) on the RSC „SKIF“ site.

• Seismic loads from moving road vehicles are recorded in the form of a continuous spectrum within a frequency range from 4 to 30 Hz. They have a typical duration of about 2 min. Due to fast attenuation, these impacts are perceptible only at the station nearest to the highway.

• Industrial noise emitted by the nearby facilities equipment are expressed by two types of monochromatic vibrations: first, with stable frequency and, second, with sliding frequency. Operating mode of the sources varies from continuous to intermittent at various frequencies. Typical long-term frequencies (during 24 hours) — 10, 13, 18 and 25 Hz. Signals at various frequencies from 30 Hz to 50 Hz occur from time to time. They are rare and last not longer than 2–3 h. Most of monochromatic signals are induced by the nearby plant and decay considerably with distance — approximately by one order per 500 m.

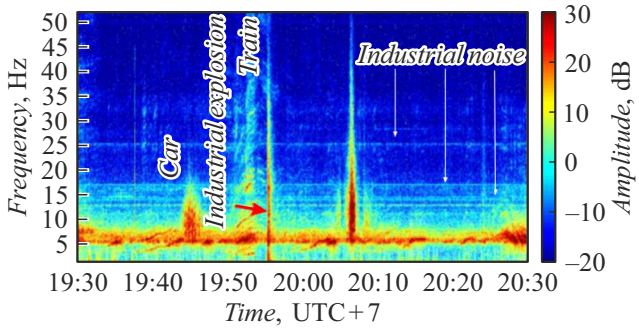

Figure 5. spectral pattern of various seismic events observed on the RSC „SKIF“ site. The amplitude is given with respect to 0.1 μm/s.

For illustration, the spectral pattern containing various signals recorded by one of RSC „SKIF“ seismic stations is shown in Figure 5.

Table 3 shows peak values or ground velocities (PGV), accelerations (PGA) and displacements (PGD) on the SKIF site for various events as well as typical spectral frequencies of such events (f), duration (t) and approximate quantity per 24 hours (N). RMS column shows rms ground displacements (for the purpose of assessment, the foundation transmission factor is taken as equal to 1).

It is shown that relevant seismic events have typical frequencies not higher than 50 Hz, earthquakes and industrial explosions occur rarely compared with the transport loads, night-time general seismic noise is much lower and no large heavy industry facilities are present near the construction site.

3. Closed beam orbit distortion due to the displacement of the SKIF storage ring magnetic components

Vertical magnetic field component on the orbit $\Delta B_y(s)$ causes excitation of the horizontal closed bean orbit that is

Figure 6. Magnet assemblies on girders for the storage ring (left) and for SKIF synchrotron [9].

described by the non-homogeneous Hill equation

$$x'' + K_x(s)x = \frac{\Delta B_y(s)}{B\rho}, \tag{3}$$

where $K_x(s)$ is the focusing coefficient, and $B\rho$ is the magnetic structure rigidity. The equation is solved as follows

$$x_{co} = \int_s^{s+C} G_x(s, s') \frac{\Delta B_y(s')}{B\rho} ds', \tag{4}$$

where the integral is taken on the accelerator perimeter of Green's function of equation (3):

$$G_x(s, s') = \frac{\sqrt{\beta_x(s)\beta_x(s')}}{2 \sin \pi\nu_x} \cos\big(\pi\nu_x - |\psi_x(s) - \psi_x(s')|\big), \tag{5}$$

where$\beta_x(s)$, $\psi_x(s)$ and $\nu_x(s)$ are betatron amplitude and phase functions and betatron frequency, respectively. Equations for the vertical motion are identical and are not shown herein.

The orbit distortion depends on various factors: type of magnet, magnet strength, betatron function at the location, etc., including the type of magnet displacement — independent or correlated in groups. Displacement of the storage ring as a whole apparently does not cause the orbit displacement and the simultaneous displacement of adjacent focusing and defocusing lenses causes lower orbit distortions than the individual displacement. Therefore, magnetic components in the SR sources shall be preferably placed on long (several meters) rigid girders(„beams“) that provide correlated displacement of the magnets attached to them (Figure 6).

Assuming the typical seismic wave velocity in the concrete foundation of the storage ring equal to $\nu \approx 3000$ m/s, it is easily found that frequencies about a thousand hertz correspond to independent magnet vibrations, frequencies equal to hundreds of hertz correspond to coherent magnet displacements on a length of several meters (girder-mounted magnets), frequencies equal to tens of hertz correspond to the displacement of the superperiod as a whole.

To estimate the effect of the transverse displacement Δx of individual types of magnetic components by the degree of closed orbit distortion x_{co}, a statistic transmission coefficient M_x is introduced (and similarly for the vertical coordinate) [10]:

$$\langle x_{co} \rangle = M_x \langle \Delta x \rangle, \tag{6}$$

where rms values are shown in angle brackets. The transmission coefficient varies with the various types of magnetic components. For example, for random displacement of quadrupole lenses for which

$$\Delta B_y = \Delta x \frac{dB_y}{dx}, \tag{7}$$

Table 4. Transmission coefficients for dipoles, quadrupoles and sextupoles with rms magnet displacement 100 nm

Quantity	M_{dip}	M_{quad}	M_{sext}	M_Σ
x	12	113	$4.2 \cdot 10^{-4}$	113
y	28	45	$2.2 \cdot 10^{-4}$	53

the following estimate may be get

$$M_x \approx \frac{\sqrt{N_q}}{2\sqrt{2}\,|\sin(\pi\nu_x)|}\,\frac{1}{B\rho}\,\frac{\overline{dB_y}}{dx}\,\overline{\beta}_x\,\overline{l}, \qquad (8)$$

where N_q is the quantity of quadrupole lenses, and the line on top shows the mean value, $\overline{l}$ is the mean length of components. When the quadrupole lens gradients and betatron function are high, then the transmission coefficient may be much higher than 1, i.e. small displacements of quadrupole lenses will cause significant distortions of the closed orbit.

We have calculated the transmission coefficient for various groups of SKIF magnetic components by setting random magnet displacements and simulating the closed orbit distortion. Since displacements induced by seismic vibrations are addressed, the rms value was assumed equal to 100 nm corresponding to train passage. Optical structure sensitivity was assessed in Accelerator Toolbox [11] and MADX [12] using the following scenario:

- Magnetic components (or series of magnets) are displaced horizontally or vertically by a random normally distributed quantity set by standard deviation $\sigma_{x,y} = \langle \Delta x, y \rangle$. The distribution is „cut off" at $\pm 3\sigma$ to avoid unrealistic high quantities.
- Closed orbit deviation is measured in the center of each straight section (at the removable device location).
- When approximately 1000 samples had been collected, rms orbit deviation was found in each observation point, and then averaging by their quantity was carried out and $\langle x, y_{co} \rangle$ was derived.
- The transmission coefficient was calculated as $M_x = \langle x_{co} \rangle / \sigma_x$ (and similarly for the vertical direction) and is shown in Table 4.

For such small displacements and taking into account the quadratic dependence of the dipole field of sextupole lenses on the displacement, it is apparent that the orbit distortion from the sextupoles is negligibly small and will be omitted hereinafter. While the maximum contribution, as has been expected, is made by strong quadrupole lenses.

Another important issue is the dependence of the closed orbit distortion on the seismic vibration wavelength or, in other words, on whether the magnetic components are displaced individually or coherently. Three cases were addressed: independent displacement of dipoles and quadrupoles from each other (Table 5), magnetic components placed on the same girder are displaced coherently, and the girder to girder is displaced independently (Table 5), and superperiod displacement as a whole: all magnetic components in the superperiod move coherently and the superperiod displacement with respect to the superperiod is independent.

Table 5. RMS orbit deviations according to the simulation data

Quantity	Specified value	Displacement case		
		Independent	Girder	Superperiod
x, μm	3.4	11.3	10.3	0.235
x', μrad	0.22	0.7	0.59	0.016
y, μm	0.4	5.5	1.74	0.288
y', μrad	0.17	2.3	0.74	0.127

In all three cases, the magnets (or series of magnets) were displaced randomly as described above with rms deviation $\sigma_{x,y} = 100$ nm. „Specified value" column shows the specified values equal to 10% of the beam sizes (space and angular) in the center off the straight section as shown in Table 2.

Table 5 shows that, though the magnets placed on girders considerably (by a factor of three) reduce the angular displacement of the SR beam in the emission point compared with the independent magnet displacement, the results still do not meet the user requirements. while the superperiod displacement, though meets the specified values, is impracticable. To improve the results, a feedback system consisting of beam position sensors (electron and synchrotron) and a set of adjusters with a bandwidth up to 1000 Hz shall be used. Such systems are common for modern SR sources[13–17].

4. Feedback system adjuster parameter estimation

Using the foregoing findings, parameters of the magnetic adjusters needed to control the beam orbit in the radiation point (center of the straight section) will be estimated in the range required to bring the data listed in Table 5 in line with the user requirements. For such estimation, the feedback system bandwidth will be assumed as endless (i.e. a static closed orbit distortion adjustment pattern is addressed now).

The SKIF storage ring has 320 dipole magnets for closed orbit adjustment. Vast majority of them is combined with sextupole lenses on whose poles additional current windings are placed to excite vertical or horizontal magnetic field. Taking into account the aluminium vacuum chamber on which the sextupole lenses are placed, the frequency range of such adjusters does not exceed several hertzs. Besides, according to Table 3, orbit stabilization due to microseismic noise requires effective operation up to several hundreds of hertzs. Therefore, it is suggested to make

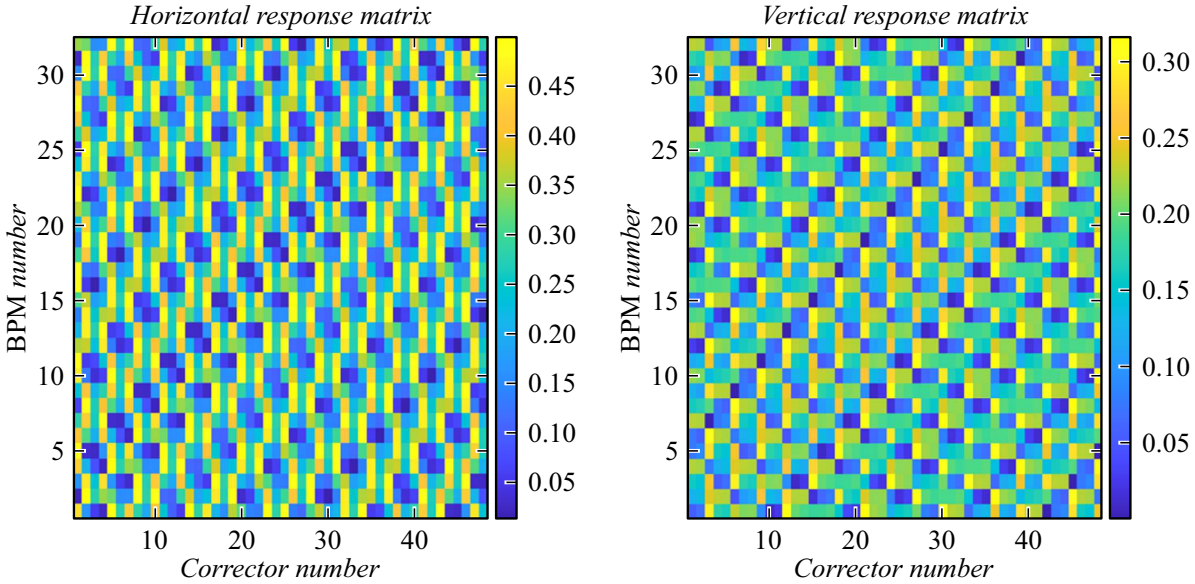

Figure 7. Response matrices. BPM — beam position monitor.

an additional wideband system for dynamic beam position correction in the point of SR emission from the undulators (in the centers of straight sections) that consists of „fast“ magnetic adjusters placed on a stainless steel thin-wall (wall thickness of 0.5 mm) vacuum tube. Due to very dense packing of the SKIF storage ring components, we place three fast adjusters per each superperiod. Figure 7 shows the response matrices where 48 adjusters are plotted on the horizontal axis, and beam position sensors nearest to the center of the section are plotted on the vertical axis (two sensors to the left and to the right of the center of each of 16 sections). Pixel color shows the degree of adjuster impact on the bean orbit on the corresponding position sensor in accordance with (2) and (3): dark color means that a strong adjuster is required to change the orbit, light color means that a weak adjuster is sufficient.

It is shown that there is a sufficient number of effective adjusters for each beam position sensor.

The closed electron beam orbit was adjusted using singular value decomposition (SVD). The adjustment included 48 magnetic adjusters (3 adjuster $\times$ 16 superperiods), each of them is intended for horizontal and vertical orbit adjustment, and 32 beam position sensors placed near the removable devices. For excitation, a case of independent magnet displacement with rms deviation equal to 100 nm was used.

Figure 8 shows bar charts of coordinate and angle distribution (horizontally and vertically) in the center of straight sections before adjustment (left row) and after adjustment (right row) for 4000 tests.

RMS values are summarized in Table 6 that shows that the offered fast feedback system is sufficient to restore the orbit displacement in the radiation points to the required position. Maximum integral adjuster values for this series of tests do not exceed 2 G $\times$ 10 cm horizontally and 1.5 G $\times$ 10 cm vertically.

Taking into account man-made seismic noise that are currently unknown such as pumps, transformers, converters, handling and loading equipment, machines, etc., that may occur at RSC „SKIF“ after commissioning, we have assumed the maximum transverse field in the adjuster 10 G

Table 6. RMS orbit deviations before after adjustment

Quantity	Specified value	Independent deviation	
		Before adjustment	After adjustment
x, μm	3.37	11.3	0.07
x', μrad	0.42	0.7	0.02
y, μm	0.22	5.5	0.07
y', μrad	0.17	2.3	0.02

Note. Column designations are identical to those in Table 5.

Table 7. Requirement for he „SKIF“ fast adjuster

Number of adjecters	48
Maximum field	$\pm$10 G
Maximum winding current	2.8 A
Effective length	10 cm
Overall length with windings	12 cm
Maximum processing frequency	1000 Hz

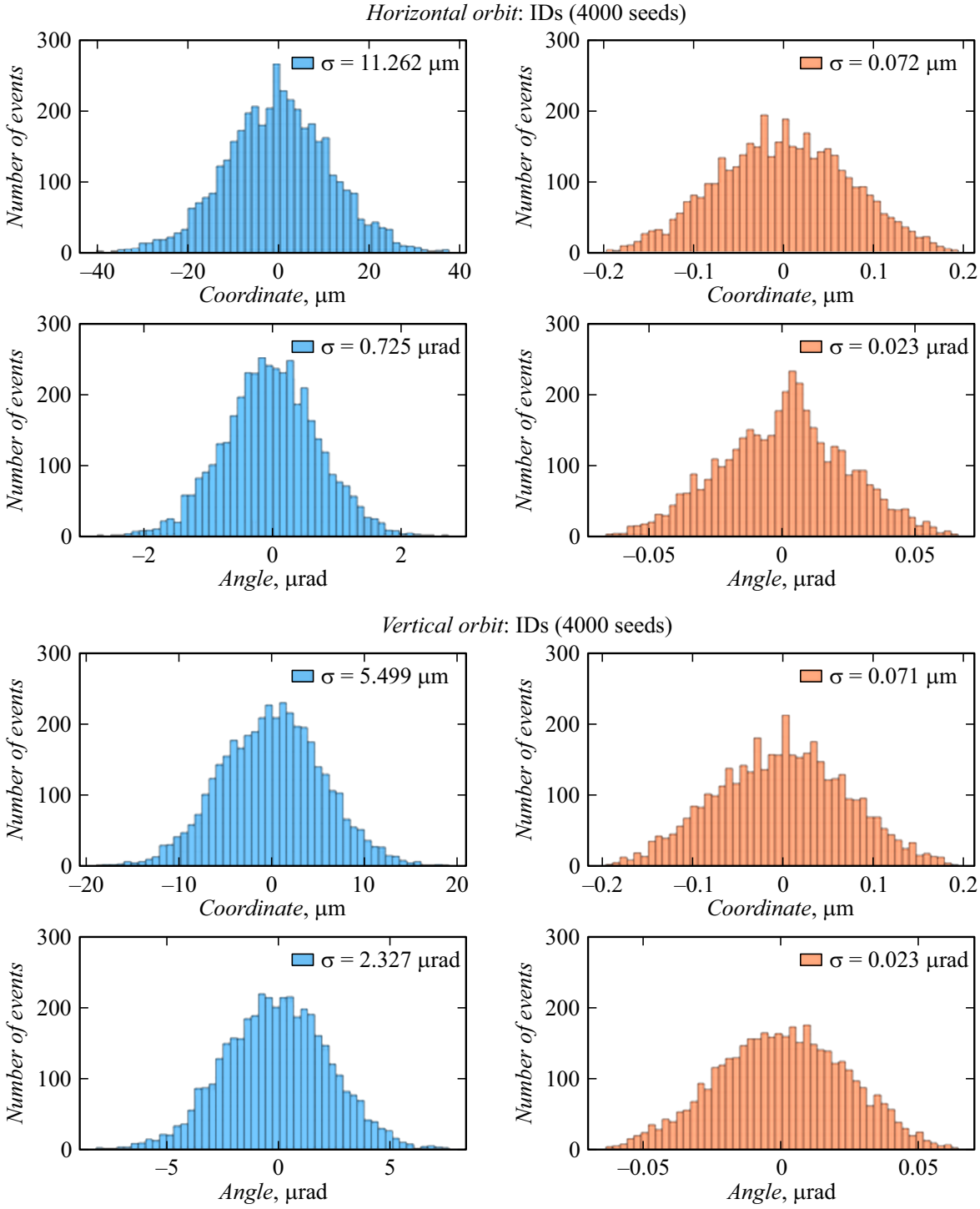

Figure 8. Simulation of orbit distortion before correction (left row) and after correction (4000 events).

with the effective length of 10 cm. Table 7 shows the fast feedback adjuster specifications.

3D model of the fast magnetic adjuster is shown in Figure 9. The magnet core is a rectangular frame made from power ferrite N87 with aperture 80 mm and four coils containing 32 copper conductor turns with cross-section 1.0×2.8 mm. Yoke length is 30 mm, lateral dimensions of magnet are 17.9×14 cm. The core design and special coil windings provide transverse uniformity of the magnetic field integral 0.5% in the aperture 10×10 mm. Calculations performed taking into account the vacuum chamber show that the chosen ferrite grade allows to achieve the magnetic field integral of $100\,\text{G} \times \text{cm}$ during linear rise of the power supply

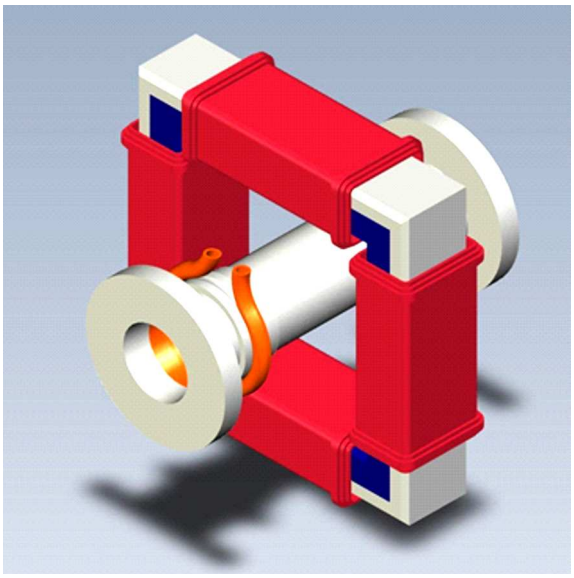

Figure 9. 3D model of fast two-axis adjuster with vacuum chamber

current from 0 to 2.8 A, that is sufficient for our objectives.

Conclusion

The effect of seismic vibrations was analyzed using the measurements made by two independent companies at RSC „SKIF“ site. Numerical simulation has shown that the measured seismic vibration level at the accelerator site may affect the closed electron beam orbit deviation considerably and exceed the SR user requirements for beam stability. To maintain the beam stability, the fast feedback system was considered, fast adjuster arrangement was chosen, adjuster parameters were estimated and magnet design was offered.

Funding

This study was supported financially by grant No. 22-27-20146 of the Russian Science Foundation and Novosibirsk Region.

Conflict of interest

The authors declare that they have no conflict of interest.

References

[1] G. Baranov, A. Bogomyagkov, I. Morozov, S. Sinyatkin, E. Levichev. Phys. Rev. Accelerator and Beams, **24**, 120704 (2021). DOI: 10.1103/PhysRevAccelBeams.24.120704
[2] D. Einfeld, J. Schaper, M. Plesko. In *Proceedings of: PAC 95 and HEACC 95* (Dallas, USA, 1995), p. 177, DOI: 10.1109/PAC.1995.504602
[3] G. Decker. *In Proceedings of DIPAC 2005* (Lyon, France, 2005), p. 233.
[4] H. Huang, J. Kay. *In Proceedings of EPAC 2006* (Edinburgh, Scotland, 2006), p. 3338.
[5] J.A. Balmer, D.J. Holder, H.L. Owen. *In Proceedings of EPAC 2000* (Vienna, Austria, 2000), p. 2328.
[6] W. Bialowons, H. Ehrlichmann. TESLA Report, **10** (2005).
[7] N. Simos, H. Amick, A. Soueid, M. Fallier. Synchrotron Radiation News, **32**, 4 (2019). DOI: 10.1080/08940886.2019.1654826
[8] A.A. Emanov, A.F. Emanov, E.B. Levichev, V.M. Solovyev, I.N. Churkin, D.G. Korabelshchikov, S.V. Sinyatkin, V.V. Yankaitis, P.A. Piminov, A.A. Bakh, G.N. Baranov, A.V. Fateev, K.Yu. Karyukina, P.O. Polyansky, A.V. Durachenko, N.A. Serezhnikov, E.A. Gladyshev, V.V. Arapov, E.V. Shevkunova, I.A. Antonov, R.A. Ershov. Seismic Instruments, **58** (6), 635 (2022). DOI: 10.3103/S0747923922060044
[9] P.A Dergach, G.N. Baranov, K.Yu. Karyukina, A.N. Drobchik. Rus. J. Geophys. Technol., **3**, 4 (2022). DOI: 10.18303/2619-563-2022-3-4
[10] L. Farvacque. *Part of Synchrotron Radiation and Free Electron Lasers* (Proceed., CERN Accelerator School, CAS, Grenoble, France, 1996), p. 287–302.
[11] Electronic media. Available at:Accelerator toollbox. https://github.com/atcollab/at
[12] Electronic media. Available at: MAD-X. https://mad.web.cern.ch/mad/
[13] Y. Tian, K. Ha, L. Yu, W. Cheng, J. DeLong, L. Dalesio, W. Levine. *In Proceed. of ICALEPCS2015* (Melbourne, Australia, 2015), p. 37, ISBN 978-3-95450-148-9
[14] Y.-R.E. Tan, T.D. Cornall, E.J. Vettoor, A. Michalczyk, N. Basten, D.J. Peake. *In Proceed. IBIC2015* (Melbourne, Australia, 2015), p. 297, ISBN 978-3-95450-176-2
[15] E. Plouviez, K. Scheidt, J. M. Koch, F. Epaud. *In Proceed. IPAC2011* (San Sebastián, Spain, 2011), p. 480.
[16] P. Leban, E. Janezic, M. Sjöström. *In Proceed. IPAC2014* (Dresden, Germany, 2014), p. 1748, DOI: 10.18429/JACoW-IPAC2014-TUPRI078
[17] L. Sanfelici, D. Tavares, D. Felix Ferreira, S. Marques, F.H. Cardoso. *In Proceed. 2011 Particle Accelerator Conference* (NY., NY., USA, 2011), p. 597.

Translated by Ego Translating